Received: 9 January 2020 | Revised: 6 March 2020 | Accepted: 14 March 2020

DOI: 10.1111/cas.14396

ORIGINAL ARTICLE

Cancer Science WILEY

Role of increased vascular permeability in chemotherapy-induced alopecia: In vivo imaging of the hair follicular microenvironment in mice

Noriko Sagawa[1] | Yusuke Oshima[1,2] | Takahiro Hiratsuka[1] | Yohei Kono[1] | Tsuyoshi Etoh[1] | Masafumi Inomata[1]

[1]Department of Gastroenterological and Pediatric Surgery, Faculty of Medicine, Oita University, Yufu, Oita, Japan

[2]Faculty of Engineering, University of Toyama, Toyama, Japan

Correspondence
Noriko Sagawa, Department of Gastroenterological and Pediatric Surgery, Oita University Faculty of Medicine, Idaigaoka 1-1, Hasama-machi, Yufu-city, Oita 879-5593, Japan.
Email: sagawanoriko@oita-u.ac.jp

Funding information
Japan Society for the Promotion of Science, Grant/Award Number: JP19K18031

Abstract

Chemotherapy-induced alopecia is one of the most difficult adverse events of cancer treatment for patients. However, it is still unknown why anticancer drugs cause hair loss. We aimed to clarify the mechanism of chemotherapy-induced alopecia in mice using an *in vivo* imaging technique with a two-photon microscope, which enables observation of the deep reaction in the living body in real time. In this study, ICR mice were injected intraperitoneally with cyclophosphamide (120 μg/g). Changes in the hair bulb morphology, subcutaneous vessel permeability, and vessel density were evaluated by two-photon microscopy and conventional methods. In order to determine whether there is a causal relationship between vascular permeability and hair loss, we combined cyclophosphamide (50 μg/g) with subcutaneous histamine. We found that the hair bulbs became smaller, blood vessels around the hair follicle decreased in diameter, and vascular permeability was confirmed by two-photon microscopy and conventional examination at 24 h after cyclophosphamide injection. Apoptosis occurred in vascular endothelial cells around the hair follicle. Additionally, hair loss was exacerbated by temporarily enhancing vascular permeability with histamine. In conclusion, cyclophosphamide caused a decrease in vascular density and an increase in vascular permeability, therefore increased vascular permeability might be one of the causes of chemotherapy-induced alopecia.

KEYWORDS

chemotherapy-induced alopecia, cyclophosphamide, *in vivo* imaging, two-photon microscopy, vascular permeability

Abbreviations: CIA, chemotherapy-induced alopecia; CYP, cyclophosphamide; EB, Evans blue; OCT, optimal cutting temperature; TRITC, tetramethylrhodamine; VEGF, vascular endothelial growth factor; vs, versus.

1 | INTRODUCTION

Chemotherapy-induced alopecia is one of the most difficult adverse events of cancer treatment for patients in clinical oncology,[1] and it has a substantial impact on patient body image. Recently, a large-scale questionnaire survey targeted Japanese patients with breast cancer who were scheduled to receive chemotherapy,[2] and the CIA incidence varied depending on the type and dose of anticancer drugs. Cyclophosphamide (CYP) is an anticancer drug that remains a key drug for cancer chemotherapy. CYP is used in chemotherapy protocols for various tumors, carcinomas, and sarcomas. It is always used in preoperative and postoperative adjuvant therapy in the treatment of breast cancer, and patients experience hair loss very frequently. There is no preventive method for CIA, and it still unknown why anticancer drugs cause hair loss. Therefore, it is urgent to clarify the mechanism of CIA.

A CIA mouse model of CYP-induced alopecia is well established, and possible mechanisms underlying hair follicular response to CYP treatment have been reported.[3-6] For instance, Botchkarev et al reported that p53 is essential for triggering apoptotic cell death in the hair follicles that is induced by CYP in mice.[7] However, we found few studies about changes in the microenvironment of hair follicles during exposure to CYP. There is only one report about reduced blood vessel density in the lower part of the bulge area because of inhibition of hair-follicle-associated angiogenesis without vascular apoptosis in doxorubicin-induced CIA.[6] Additionally, no study has focused on microenvironmental dynamics around hair follicles in a CYP-induced CIA model. In most animal studies of CIA, dorsal skin tissues are harvested from euthanized mice, but this approach is often insufficient to verify the biological properties. We hypothesized that exposing the hair follicles to CYP leads to dysfunction of hair growth, resulting in changes in the local microenvironment including blood flow, vascular structure, and permeability. However, there is no direct *in vivo* study to show real time insights of the microenvironmental dynamics around hair follicles. Two-photon microscopy has been developed and is widely used in the biomedical research field; it enables observation of the deep reaction in the living body in real time and is useful for elucidating the mechanism of biological phenomena. In this study, we aimed to determine the mechanism of CYP-induced CIA in mice by employing an *in vivo* imaging technique using the two-photon microscope.

2 | MATERIALS AND METHODS

2.1 | Animal model

Six-wk-old female ICR mice were purchased from Japan SLC, Inc (Shizuoka, Japan). Mice were housed in a temperature-controlled space with 12 h of light daily, and were fed freely on food and water. Fifty-eight mice were used in this study. All experimental procedures were approved by the Institutional Animal Care and Use Committee of Oita University, Faculty of Medicine (approval number: 182 001).

2.2 | Induction of anagen and alopecia

Anagen was induced in the dorsal skin of mice in telogen of the hair cycle by depilation. Depilation was performed by gently shaving the mice with clippers and applying a melted wax/rosin mixture under general anesthesia, as described previously.[8] After hardening, it was peeled off from caudal to cranial direction. Then all telogen hair shafts were plucked, which induces the predictable and highly synchronized development of anagen follicles that are morphologically indistinguishable from spontaneous anagen follicles. On day 9 post depilation, it becomes a model mouse adapted to the human hair cycle. Alopecia was induced by intraperitoneal administration of CYP and subjected to in vivo imaging and further analyses.

2.3 | Two-photon microscopy

For the *in vivo* imaging protocol, we divided the mice into two groups: CYP 120 μg/g (CYP120), as CYP120 group, or PBS; as control group. In 24 h after administration, we harvested the skin flap and turned it over with the mice under general anesthesia and observed the subcutaneous tissue from the internal side using an upright two-photon excitation fluorescence microscopy system (A1RMP, Nikon Corporation, Tokyo, Japan). We first injected 100 μg/100 μL Texas-red® labeled *Lycopersicon esculentum* lectin (TL-1176, Vector Laboratories, Burlingame, CA, USA) into the tail vein to visualize and evaluate the perifollicular vessels, and then 150-μg TRITC-conjugated 70-kDa dextran (D-1819, Life Technologies Corporation, Eugene, OR, USA) and 150-μg FITC-conjugated 150-kDa dextran (FD150S-1G, Sigma-Aldrich, St. Louis, MO, USA) were dissolved in 100 μL of PBS to evaluate leakage into the subcutaneous interstitial tissue. We performed two-photon excited fluorescence imaging with a ×25 water-immersion objective lens (CFI75 Apo 25xW MP, numerical aperture = 1.1; Nikon) using an ultrafast tunable laser (Chameleon Discovery NX, Coherent Inc, Santa Clara, CA, USA) (excitation, 950 nm; repetition rate, 80 MHz; pulse width, 100 fs). We placed emission filters at 525/50 nm (center wavelength/bandwidth) to obtain the fluorescence signal of FITC, an emission filter at 575/50 nm for the fluorescence signal of TRITC, and a dichroic mirror at 593 nm to isolate the fluorescence signal of Texas-red®. We also used a short-pass filter at 492 nm to obtain a second harmonic generation signal from the collagen fibril.

2.4 | Vascular permeability test

We used the Miles assay to evaluate the vascular permeability *in vivo* as follows. Mice were put in the fixing device at 0, 12, or 24 h after injection of CYP120 or PBS (CYP120: five in each group, PBS: three in each group) intraperitoneally, and 0.5% EB solution (200 μL) was injected into the tail vein. Mice were sacrificed by cervical dislocation at 30 min after injection of the EB solution. Dorsal full thickness skins were collected, weighted, and minced with scissors. Each

sample was immersed in 500 μl formamide, incubated at 55°C for 48 h using a filtering process with a 100-μm cell strainer, and centrifuged at 9200 *g* for 5 min. The supernatants were collected, and absorbance was determined at 610 nm.

2.5 | Immunofluorescence and TUNEL staining

The mice were sacrificed 24 h after administration of CYP120 or PBS, dorsal skins were collected, fixed in 10% buffered formalin for 24 h, and embedded in paraffin. For immunofluorescence detection and quantification of apoptotic endothelial cells in mouse skin sections, we used a TUNEL staining kit (In Situ Cell Death Detection Kit; Roche Diagnostics, Mannheim, Germany) in combination with immunofluorescence for CD31. Skin sections were TUNEL-stained by protocol, and subsequently incubated with a rabbit polyclonal anti-CD31 antibody (1:40 dilution, ab28364, Abcam plc, Cambridge, UK) overnight at 4°C. The CD31 immunoreaction was revealed using the Alexa 594 donkey antirabbit IgG (1:400 dilution, 2 066 086, Life Technologies, Eugene, OR, USA). The slides were counterstained with DAPI (Thermo Fisher Scientific, Waltham, MA, USA). The TUNEL-positive cell counts per hair follicular were calculated.

2.6 | Evaluation of subcutaneous vascular density

Back skin from mice used in the immunostaining experiment was cryopreserved in a −80°C OCT compound. OCT compound-embedded sections (9-μm thick) were incubated overnight at 4°C with anti-CD31 antibody, and were incubated with Alexa Fluor-594-conjugated donkey antirabbit IgG for 30 min at room temperature in the dark. The slides were counterstained with DAPI. Images that were obtained from the fluorescence microscope (BZ-9000, Keyence, Osaka, Japan) were analyzed by using the application for image analysis, the public domain software ImageJ version 1.46r (National Institutes of Health, http://rsbweb.nih.gov/ij/). In the PBS and CYP groups, the evaluation was performed in four random fields of three mice each. The CD31-positive cell area per subcutaneous area was calculated.

2.7 | Vascular hyperpermeability model with histamine

In order to examine whether increased vascular permeability is involved in CIA, the other experimental protocol was conducted by temporarily enhancing vascular permeability with histamine (His). Twenty-four mice were divided into four groups, six mice in each group: CYP 50 μg/g (CYP50) + His sc, CYP 50 + PBS sc, PBS + His sc, and PBS + PBS sc, wherein CYP50 or PBS was administered intraperitoneally, and then His or PBS was administered subcutaneously. The mice induced into anagen received CYP50 or the same amount of PBS. From 1 h to 2 h after administration, mice received a continuous subcutaneous injection (3000 μg/600 μL/1 h) of histamine or PBS under the dorsal skin while under general anesthesia. After 24 h, three mice in each group were sacrificed and the tissues were collected. The others were remained alive and were observed for hair loss 6 d later.

2.8 | Statistical analysis

All data are presented as mean ± standard deviation. Student *t* test for nonrelated samples was used for statistical analysis. The results were analyzed by using SPSS for Windows version 25 (IBM Corp., Armonk, NY, USA). The results were considered significant if the *P*-value was < 0.05. A two-way ANOVA along with the post hoc Bonferroni test was applied to the data to determine the interaction and relationship between CYP or PBS injection and time after administration in vessel permeability.

3 | RESULTS

3.1 | Optimal mice model for observation around hair follicle by two-photon microscopy

First of all, the optimal model for observing hair follicles with a two-photon microscope was examined. C57BL/6 mice were considered to be suitable for the CIA model, because hair in C57BL/6 mice is black and suitable for detecting changes in the dorsal skin color. However, endogenous chromophores interfered seriously with two-photon microscopy (Figure 1A,B). Therefore, we used albino ICR mice instead of C57BL/6 mice. In addition, as the approach from the epidermis side did not allow sufficient observation of the hair follicle part, it was decided to observe from the back side, and we designed a murine dorsal flap model. This axial pattern skin flap was harvested based on the caudal dorsal artery.

3.2 | Changes in dermal microenvironment around hair follicles by CYP

To observe morphological changes in the hair follicle and the surrounding microenvironment caused by administration of CYP, living mice were observed with a two-photon microscope. Figure 2 shows the two-photon excited fluorescence images obtained from the CYP120 group and the control group at 24 h after injection represented by multicolor images. In the field of view, the histological structure of hair bulbs and microvessels was shown on the back of subcutaneous structures including adipocytes and connective tissue (Figure 2A,B). The single-color images of the vascular observation are shown in Figure 2C,D. These corresponding anatomical drawings are shown in Figure 2E,F. In the control group, many microvessels surrounded the hair follicle (Figure 2A,C). In contrast, in the CYP120 group, there were fewer but more unclear microvessels, and the size of the hair follicles

seemed be smaller than that in the control group (Figure 2B,D). Furthermore, the accumulation of granules (particle structures emitting autofluorescence) was observed in the hair bulbs (Figure 2B). Those morphological changes and increased autofluorescence signals in the hair follicles were obvious in the CYP120 group compared with control group. To confirm the morphological alterations observed in two-photon microscopy, we generated the tissue section and quantified the subcutaneous thickness and the hair bulb size. Histologically, the hair bulbs became smaller and the subcutaneous layer was thinner at 24 h after CYP120 treatment (Figure 3A,B). The maximum diameter of the hair bulb was significantly smaller (59.9 ± 13.1 μm vs 109.0 ± 23.1 μm,

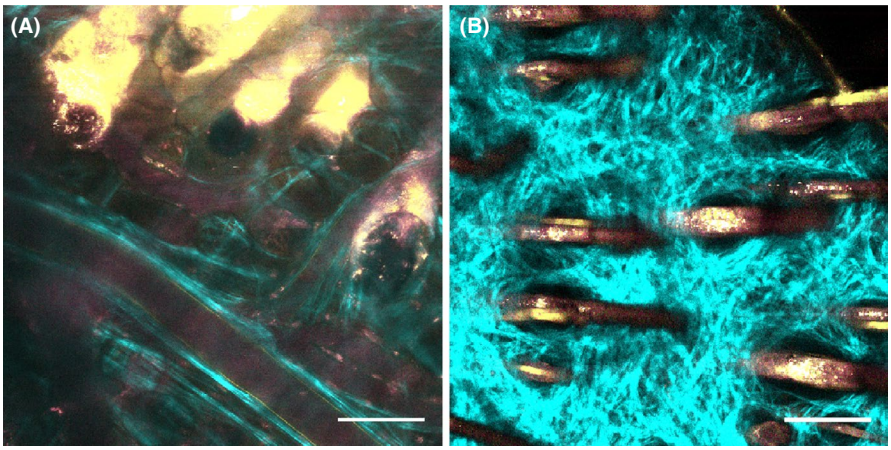

FIGURE 1 The C57BL/6 mouse is not suitable for *in vivo* observation using two-photon microscopy. Two-photon images obtained from the dorsal skin flap of a C57BL/6 mouse. A, Snapshot view of the hair follicular circumference taken from the internal side. B, Snapshot view of the hair shaft taken from the surface. Strong autofluorescence signals are observed in the hair follicle surroundings and the hairs burned by laser absorption during image acquisition. The scale bars represent 100 μm

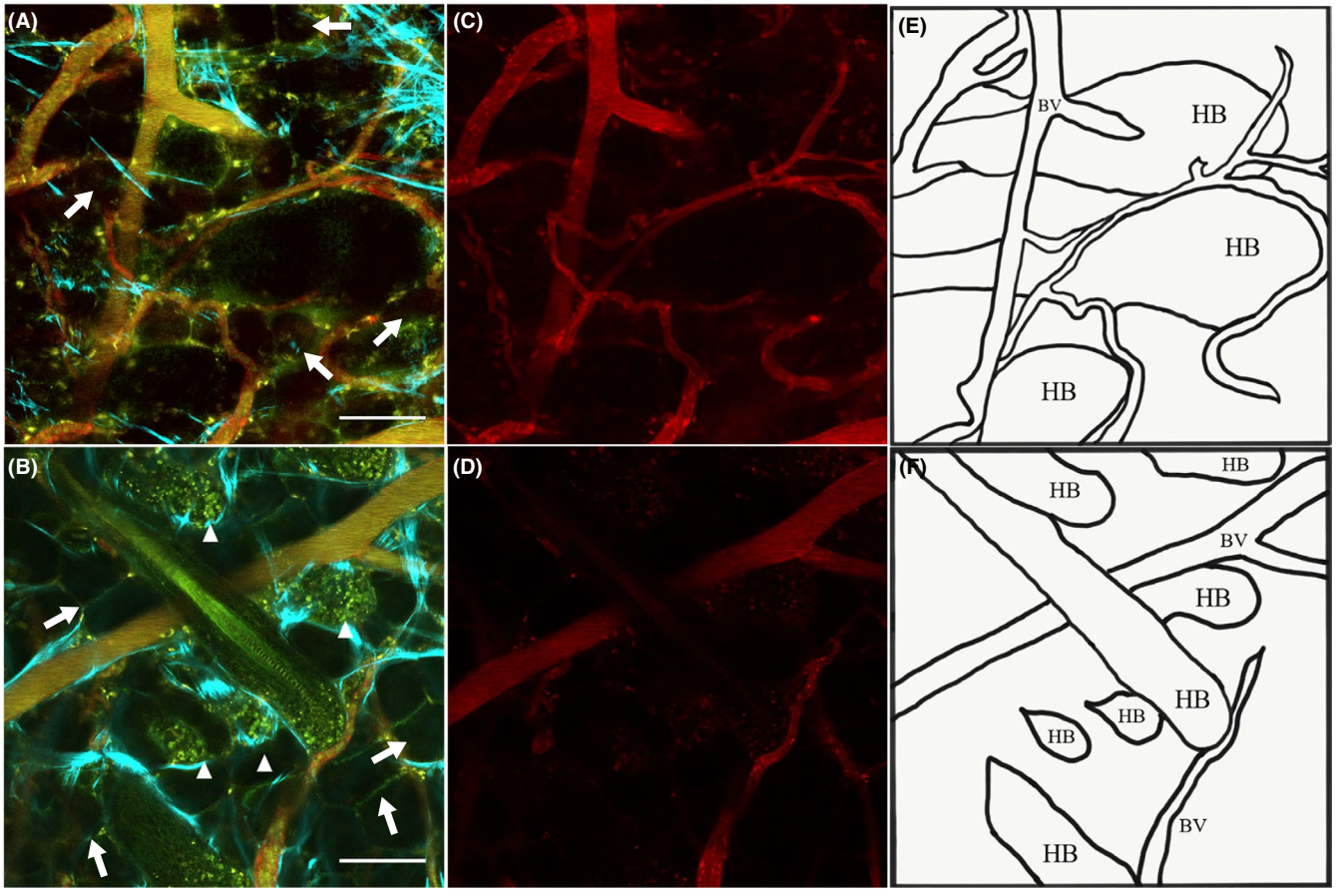

FIGURE 2 Microenvironment around hair follicle 24 h after CYP120 using two-photon microscopy. The dorsal skin flap of the mice is observed by two-photon microscopy at 24 h after cyclophosphamide 120 μg/g (CYP120) injection (lower panels) and the control group (upper panels). A, B, Snapshot images merged with all colors: cyan, second harmonic generation from collagen fibrils; green, autofluorescence from intrinsic substances; red, Texas-red® fluorescence from the vessel wall. C, D, Single-color images with Texas-red® fluorescence. E, F, The corresponding anatomical drawings (HB: hair bulb; BV: blood vessels). White arrowheads indicate small granules and white arrows indicate adipocytes. The scale bars represent 50 μm

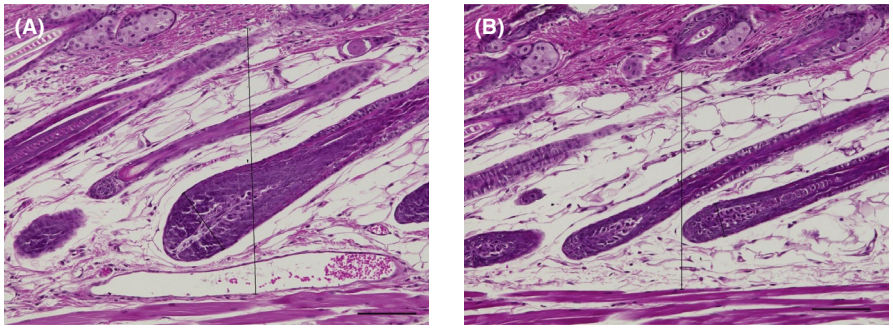

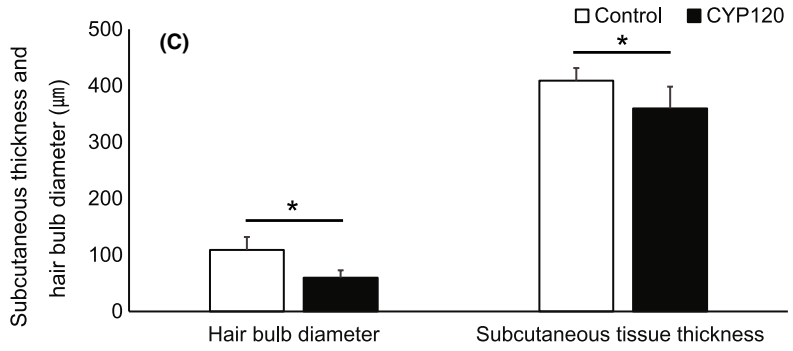

FIGURE 3 Changes in subcutaneous tissue at 24 h after CYP 120. Representative histological images obtained from (A) the PBS group, and (B) the CYP120 group. The thickness of the subcutaneous tissue is determined from the lower end of the dermis to the upper end of the fascia, and the maximum value in the visual field is measured. The size of the hair bulb is measured at the site where the largest split surface has the largest diameter. The scale bars represent 100 μm. C, The subcutaneous tissue thickness and the maximum diameter of the hair follicular were measured in at least four random visual fields in each group (n = 3). Data are presented as mean ± standard deviation. Student *t* test was used for statistical analysis (*$P < .05$)

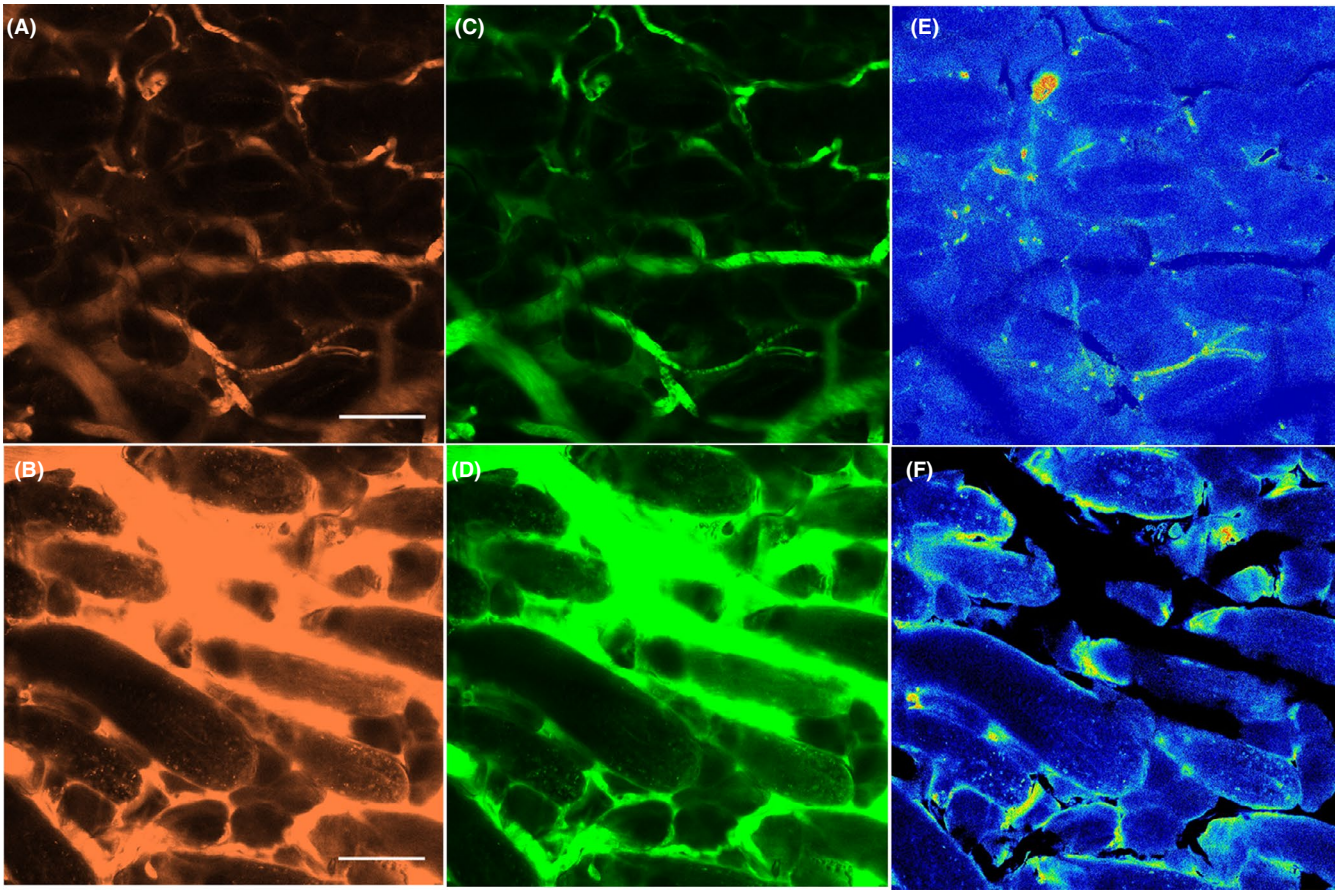

FIGURE 4 Changes in vascular permeability caused by CYP 120 with two-photon microscopy. Contrast images of fluorescent tracers with different molecular weights at 24 h after CYP120 injection (lower panels) are shown and compared with the control, PBS injection (upper panels) by using two-photon microscopy. Snapshot images of dorsal skin from mice are taken with two different colors: A, B, orange, for tetramethylrhodamine (TRITC) florescence bound to the 70-kDa dextran; C, D, green, for FITC fluorescence bound to the 150-kDa dextran; E, F, subtraction images obtained by subtracting the 150-kDa dextran image from the 70-kDa dextran image (orange-green). The scale bars represent 50 μm

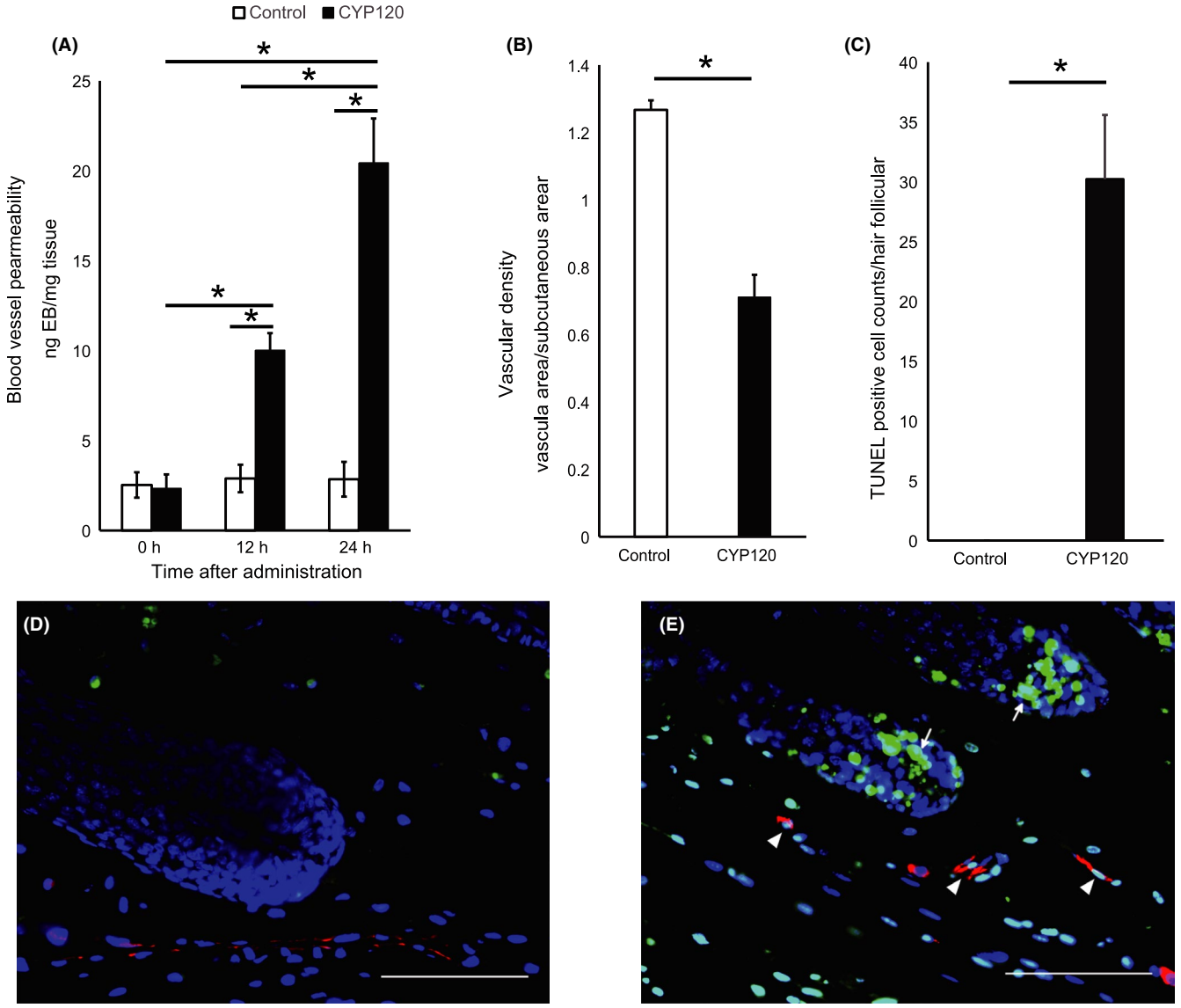

FIGURE 5 Morphological changes in subcutaneous tissue by CYP120. A, Changes in vascular permeability over time. The vascular permeability of the mice back at 0, 12, and 24 h after the CYP120 (n = 5) or PBS (n = 3) administration was evaluated by Miles Assay. Data are presented as mean ± standard deviation (*P[>*F*] < .05, the interaction was significant in post hoc tests after ANOVA). B, Changes in vascular density. Twenty-four hours after CYP120 or PBS administration, the back of the mouse was double-stained with CD31 and DAPI. The CD31-positive area per subcutaneous area of each sample (n = 3) was calculated using image analysis software. Student *t* test was used for statistical analysis (**P* < .05). C, Number of TUNEL-positive cells in hair follicle. Twenty-four hours after administration, triple staining was performed with CD31, TUNEL, and DAPI. TUNEL-positive cells per hair follicle were counted in three or more visual fields of each (n = 3) and statistically examined (**P* < .05). The triple staining of hair follicles and blood vessels obtained from (D) PBS and (E) CYP120 injection, respectively. White arrows and arrowheads indicate TUNEL-positive cells in hair follicular and in vascular endothelium, respectively. TUNEL, indicated with green; CD31, red; and DAPI, blue. The scale bars represent 100 μm

P < .001) and the subcutaneous tissue was also significantly thinner (359.8 ± 38.5 μm vs 408.9 ± 22.6 μm, *P* < .05) in the CYP120 group than in the control (Figure 3C).

3.3 | Evaluation of vascular permeability using tracers

Next, we evaluated the functional changes in blood vessels around the hair follicle by using two types of contrast agents with different molecular weight after administration of CYP120 in living mice. Most of both tracers were retained within the microvascular structure in the control (Figure 4A,C). The subtraction image (Figure 4E) was obtained by subtracting the FITC image data from TRITC image data, and was displayed as a pseudocolor image. The signal distribution of the subtraction image indicated that the 70-kDa dextran was delivered to the finer blood vessels and could slightly leak into the interstitial space in the control mice (Figure 4E). However, in the CYP120 group, both large and small tracers drastically flowed out into the interstitial space around the hair bulbs (Figure 4B,D). Moreover, we

found that the shape of hair bulbs was clearly depicted in the subtraction image because the small tracer could spread inside the hair follicles of the CYP120 group (Figure 4F).

3.4 | CYP treatment-induced vascular hyperpermeability and microvascular disorder

Quantitative evaluation of the vascular hyperpermeability was performed by Miles assay. No change in vascular permeability was observed in the control group: 0 h after injection, 2.53 ± 0.70 ng/mg skin; 12 h after injection, 2.89 ± 0.76 ng/mg skin; and 24 h after injection, 2.85 ± 0.96 ng/mg skin. In the CYP120 group, the concentration of EB increased over time: 0 h after injection, 2.35 ± 0.87 ng/mg skin; 12 h after injection, 10.03 ± 1.05 ng/mg skin; and 24 h after injection, 20.44 ± 2.75 ng/mg skin. There were significant differences between 0-12 h, 0-24 h, 12-24 h in the CYP120 group, CYP120 - Control at 12 h, and CYP120 - Control at 24 h, respectively (Figure 5A). Furthermore, to confirm the microvascular disorder revealed by two-photon microscopy, the triple staining with CD31, TUNEL, and DAPI was performed in the tissue section as shown in Figure 5B-E. CYP120 administration affected not only vessel permeability but also the distribution of microvascular around the hair follicles (Figure 5D,E). In the CYP120 group, the subcutaneous vessel density that was defined as a ratio of CD31-positive area/subcutaneous area was obviously less than that in the control group (Figure S1A,B). We then calculated the subcutaneous blood vessel density based on the immunofluorescent images. The blood vessel densities in the CYP120 and Control groups were 0.71 ± 0.07 and 1.27 ± 0.03 at 24 h, respectively (Figure 5B). We also examined apoptosis in the hair follicular bulbs. In the control group, TUNEL-positive cells were not detected in the blood vessels and hair follicles (Figure 5D). In contrast, in the CYP120 group, TUNEL-positive cells were detected (Figure 5E). The number of TUNEL-positive cells in the hair follicles was significantly higher than that in the control group (Figure 5C), and were found more in the lower part of the hair follicle than in the middle part of the hair follicle (Figure 5E). The TUNEL signal merged with DAPI staining was also localized on the vascular endothelium.

3.5 | Transient hyperpermeability caused apoptosis in vascular endothelial cells

The results of two-photon microscopy, Miles assay, and the histological examination showed that CYP120 administration increased vascular permeability in the hair follicle microenvironment. To investigate whether the increased vascular permeability is involved in the mechanism of the hair loss, we conducted the other experimental protocol for the administration of low dose CYP (CYP50), which does not cause hair loss and histamine, and which has a temporary vascular hyperpermeability effect. At 6 d after the administration of CYP50 or PBS combined with subcutaneous injection of histamine or PBS, no apparent hair loss was observed in the CYP50 + PBS sc (Figure S2A), PBS + His sc, and PBS + PBS sc groups. However, mice in the CYP50 + His sc group had mild hair loss compared with those in the other groups (Figure S2B). As a result of TUNEL staining of the tissue collected at 24 h after administration, TUNEL-positive cells were observed in the hair bulb of the CYP50 + His sc group (Figure 6B) but not in the other groups (Figure 6A; CYP50 + PBS sc group). The number of TUNEL-positive cells per hair follicular was

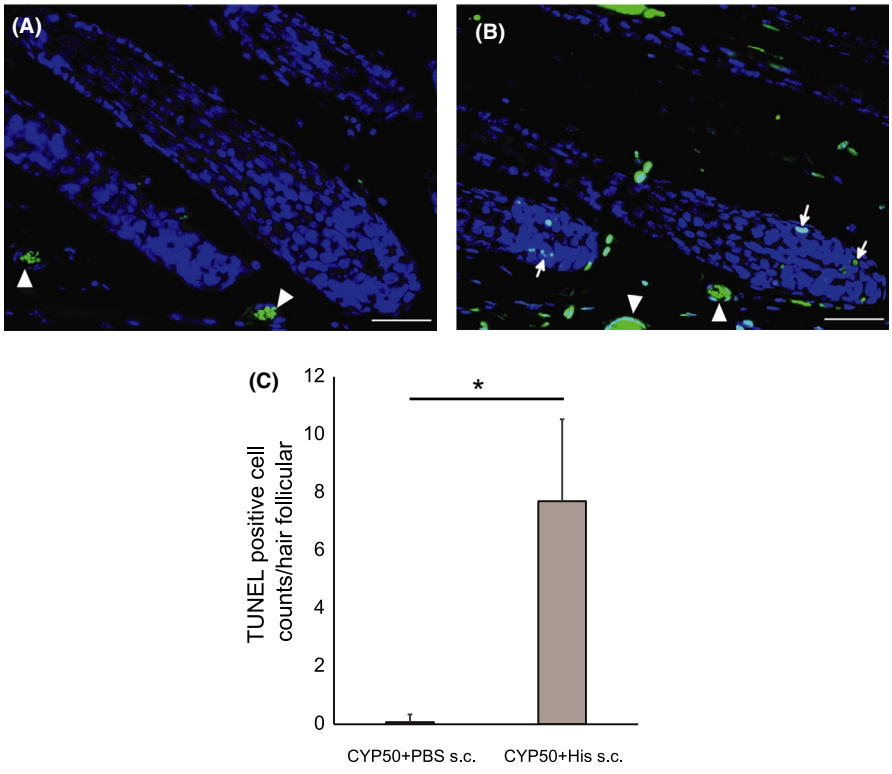

FIGURE 6 Apoptosis occurs in hair follicles when histamine sc is added to CYP50. Representative images of TUNEL and DAPI staining of subcutaneous tissue at 24 h after (A), CYP 50 μg/g (CYP50) + PBS subcutaneous injection (sc) and (B), CYP50 + histamine 3000 μg/h sc. White arrows indicate TUNEL-positive cells in hair follicles and white arrowheads indicate possible red blood cells because they are DAPI-negative. The scale bars represent 50 μm. C, TUNEL-positive cells per hair follicle were counted in three or more visual fields of each specimen (n = 3), and statistically examined (*$P < .05$)

significantly higher in the CYP50 + His sc group than in the CYP 50 + PBS sc group (Figure 6C).

4 | DISCUSSION

Intravital observation of the CIA-induced mice revealed that the microenvironment around hair follicles was drastically changed by anticancer drug administration that affected vascular permeability around the hair follicles, coinciding with a defect of the microvascular structure. Herein, we demonstrated a pivotal mechanism of CIA dynamics using a two-photon microscope with more reliable approaches to confirm those findings in *in vivo* imaging. To our knowledge, this is the first study that shows the relationship between vascular permeability and CIA by in vivo imaging.

It is noteworthy that CYP, the most commonly used drug for cancer chemotherapy, increased subcutaneous vascular permeability, and decreased the subcutaneous blood vessels in this study. Few CIA studies focused on microenvironments. However, there are various reports on the effects of CYP on blood vessels; it has a higher sensitivity to vascular endothelial cells than keratinocytes and fibroblasts,[9] damages ovarian blood vessels, and thickens the vascular wall. CYP can cause infertility[10,11] and normalize abnormal blood vessels in collagen diseases.[12,13] Although CYP enhances vascular permeability of tumors[14] and bladders,[15] there has been no previous study on the relationship between vascular permeability and CIA. The direct evidence of CYP-mediated hyperpermeability was provided by the Miles assay.[16] The Miles assay can quantify the cumulative amount of dye leakage during the time from EB administration to animal sacrifice and, as EB binds to albumin in plasma, it reflects only the permeability of albumin, approximately 66 kDa. An alternative, reliable method for observing vascular permeability in living animals using fluorescent tracers by two-photon microscopy[17] is to visually capture the vascular permeability on the region of interests. The result of two-photon imaging with florescent tracers conjugated with 70-kDa and 150-kDa dextran strongly suggests that the increased vascular permeability drastically changes the microenvironment of hair follicles and pharmacokinetics.

Two-photon microscopy and conventional methods also confirmed the decrease in blood vessel density. It can be concluded that the total volume of subcutaneous vessels was significantly reduced at 24 h after CYP 120 μg/g injection because of the decrease in vessel density and decrease in subcutaneous thickness. More apoptosis occurred in the lower part of the hair follicle than in the middle part of the hair follicle. One reason for this is that the lower part of the hair follicle could be highly sensitive to CYP because the cell division is more active at the lower part of the hair follicle than at the middle part in anagen. Another reason for this is that the lower part has fewer blood vessels and is more susceptible to vascular damage due to CYP than the middle part, which forms the vascular plexus.[18] We also confirmed that the increased vascular permeability is dominantly associated with inducing apoptosis in hair follicular cells and the hair loss by using histamine as an adjunct to CYP. Histamine is fast acting, has a very short half-life of only a few minutes, and causes a temporary increase in vascular permeability. The blood concentration of CYP is highest at 1 h after administration,[19] so histamine was subcutaneously injected from 1 h to 2 h after CYP50 injection in this experiment. In our study, TUNEL-positive cells were scattered in the hair bulbs and surrounding supporting tissues in the CYP50 + His sc group, whereas TUNEL-positive cells were not found in the CYP50 + PBS sc group. This change in the number of TUNEL-positive cells is considered to be consistent with the macrophotograph showing hair loss. By enhancing vascular permeability with His, the situation in which apoptosis did not occur originally changed to a situation in which apoptosis did occur. This situation might be caused by leakage of a large amount of CYP to the hair bulb and surrounding stroma. The possible mechanism in CYP-induced alopecia is that the anticancer agent itself changes the microenvironment of the blood vessels surrounding the hair follicle, and then the vascular permeability increases and the hair bulbs are damaged. Consequently, a vascular disorder develops, and the ischemia affects hair loss and growth.

Increased vascular permeability is one cause of CIA, assuming that the hair loss became prominent in the condition of hyperpermeability due to chemotherapy. The frequency of causing hair loss varies clinically depending on the anticancer agent and dose used. Although no epidemiological survey for the individual difference in the dose and hair loss has been conducted, the state of blood vessels in the patient's scalp is considered to be one cause. There might be risk factors of CIA, for example it might occur when a patient has an inflammatory lesion such as seborrheic eczema or a fragile vascular condition. Currently, only the scalp-cooling device is effective to some extent as CIA prevention and has been clinically applied.[20,21] There are two known mechanisms of CIA prevention by the scalp-cooling method: to inhibit the anticancer drug itself from reaching the peripheral blood vessels of the scalp by contracting the blood vessel, and to attenuate the action of the anticancer drug by deviating from the optimal temperature of the action of the anticancer drug. There is no study on the relationship between scalp cooling itself and vascular permeability, but cooling reduces vascular permeability and vascular hyperpermeability, which is caused by histamine.[22,23]If scalp cooling can reduce scalp vascular permeability due to anticancer agents, decreased vascular permeability might be a new third mechanism of CIA prevention by scalp cooling.

From the future perspective on preventing CIA, the local administration of a vascular permeability reducer and vascular endothelial cell protective agent could be effective. However, physicians should be cautious of systemic administration because this might diminish the antitumor effect, which is the original purpose of anticancer drug usage. As for anti-angiogenic therapy in clinical application with chemotherapy, bevacizumab, an anti-VEGF antibody, has been reported to decrease vascular permeability [24,25] and VEGF to enhance it.[26] VEGF is also known as one of the hair growth factors,[27] and it has been reported that VEGF itself and a component that activates VEGF are effective as a therapeutic agent for alopecia areata, non-scarring alopecia, and androgenic

alopecia.[28-30] Although there have been no reports of association between anti-VEGF antibody and CIA, it is reported that hair loss was more frequent in a bevacizumab-plus regimen than in a regimen without bevacizumab (67% vs 48%) in a clinical trial.[31] Although bevacizumab exhibits attenuated vascular permeability, its original effects of inhibiting angiogenesis may promote hair loss by anticancer agents.

In this study, there are several limitations. Firstly, in order to confirm that decreased permeability could prevent CIA, it is necessary to examine the presence of decreased hair loss with drug that reduce vascular permeability or in transgenic mice with decreased vascular permeability. Secondly, it is also necessary to verify whether other anticancer agents that induce alopecia increase vascular permeability.

In conclusion, we observed decreased blood vessel volume and increased vascular permeability in a mouse model of CIA induced by CYP. Increased vascular permeability might be one of the causes of CIA.

ACKNOWLEDGMENTS

We thank Yuiko Aso, Mayumi Wada, and Yoko Miyanari for their valuable assistance, Yoshihiro Tsumura and Toshio Ito for academic advice associated with alopecia and Mutsuhiro Takekawa and Noriko Nishizumi Tokai for their productive discussions and technical support with two-photon microscopy in the Imaging Core Laboratory, The Institute of Medical Science, The University of Tokyo. This work was supported by JSPS KAKENHI grant number JP19K18031 and the Grant for Joint Research Project of The Institute of Medical Science, The University of Tokyo.

CONFLICT OF INTEREST

Noriko Sagawa, Yusuke Oshima, Takahiro Hiratsuka, Yohei Kono, Tsuyoshi Etoh, and Masafumi Inomata received a research grant from Aderans Co., Ltd.

AUTHORS' CONTRIBUTION

NS and YO carried out the experiment. NS and YO wrote the manuscript with support from TH and YK. NS, YO, and TE analyzed the data. MI supervised this project. All authors discussed the results and contributed to the final manuscript.

ORCID

Noriko Sagawa https://orcid.org/0000-0002-4517-5061
Yusuke Oshima https://orcid.org/0000-0002-2304-8600
Takahiro Hiratsuka https://orcid.org/0000-0002-6483-6013
Masafumi Inomata https://orcid.org/0000-0002-8475-3688

REFERENCES

1. Lemieux J, Maunsell E, Provencher L. Chemotherapy-induced alopecia and effects on quality of life among women with breast cancer: a literature review. *Psychooncology*. 2008;17:317-328.
2. Watanabe T, Yagata H, Saito M, et al. A multicenter survey of temporal changes in chemotherapy-induced hair loss in breast cancer patients. *PLoS ONE*. 2019;14:e0208118.
3. Paus R, Haslam IS, Sharov AA, Botchkarev VA. Pathobiology of chemotherapy-induced hair loss. *Lancet Oncol*. 2013;14:e50-e59.
4. Hendrix S, Handjiski B, Peters EM, Paus R. A guide to assessing damage response pathways of the hair follicle: lessons from cyclophosphamide-induced alopecia in mice. *J Invest Dermatol*. 2005;125:42-51.
5. Chen SS, Zhang Y, Lu QL, Lin Z, Zhao Y. Preventive effects of cedrol against alopecia in cyclophosphamide-treated mice. *Environ Toxicol Pharmacol*. 2016;46:270-276.
6. Amoh Y, Li L, Katsuoka K, Hoffman RM. Chemotherapy targets the hair-follicle vascular network but not the stem cells. *J Invest Dermatol*. 2007;127:11-15.
7. Botchkarev VA, Komarova EA, Siebenhaar F, et al. p53 is essential for chemotherapy-induced hair loss. *Cancer Res*. 2000;60:5002-5006.
8. Paus R, Handjiski B, Eichmüller S, Czarnetzki BM. Chemotherapy-induced alopecia in mice. Induction by cyclophosphamide, inhibition by cyclosporine A, and modulation by dexamethasone. *Am J Pathol*. 1994;144:719-734.
9. Ohtani T, Nakamura T, Toda K, Furukawa F. Cyclophosphamide enhances TNF-alpha-induced apoptotic cell death in murine vascular endothelial cell. *FEBS Lett*. 2006;580:1597-1600.
10. Pascuali N, Scotti L, Di Pietro M, et al. Ceramide-1-phosphate has protective properties against cyclophosphamide-induced ovarian damage in a mice model of premature ovarian failure. *Hum Reprod*. 2018;33:844-859.
11. Ezoe K, Murata N, Yabuuchi A, et al. Long-term adverse effects of cyclophosphamide on follicular growth and angiogenesis in mouse ovaries. *Reprod Biol*. 2014;14:238-242.
12. Caramaschi P, Volpe A, Pieropan S, et al. Cyclophosphamide treatment improves microvessel damage in systemic sclerosis. *Clin Rheumatol*. 2009;28:391-395.
13. Borghini A, Manetti M, Nacci F, et al. Systemic sclerosis sera impair angiogenic performance of dermal microvascular endothelial cells: therapeutic implications of cyclophosphamide. *PLoS ONE*. 2015;10:e0130166.
14. Braunschweiger PG. Effect of cyclophosphamide on the pathophysiology of RIF-1 solid tumors. *Cancer Res*. 1988;48:4206-4210.
15. Chow YC, Yang S, Huang CJ, et al. Epinephrine promotes hemostasis in rats with cyclophosphamide-induced hemorrhagic cystitis. *Urology*. 2006;67:636-641.
16. Radu M, Chernoff J. An in vivo assay to test blood vessel permeability. *J Vis Exp*. 2013;73:e50062.
17. Egawa G, Nakamizo S, Natsuaki Y, et al. Intravital analysis of vascular permeability in mice using two-photon microscopy. *Sci Rep*. 2013;3:1932.
18. Montagna W, Ellis RA. Histology and cytochemistry of human skin. XIII. The blood supply of the hair follicle. *J Natl Cancer Inst*. 1957;19:451-463.
19. Begg AC, Smith KA. A bioassay for cyclophosphamide in blood, lung and tumour. *Br J Cancer*. 1984;49:49-55.
20. Nangia J, Wang T, Osborne C, et al. Effect of a scalp cooling device on alopecia in women undergoing chemotherapy for breast cancer: the SCALP randomized clinical trial. *JAMA*. 2017;317:596-605.
21. Smetanay K, Junio P, Feisst M, et al. COOLHAIR: a prospective randomized trial to investigate the efficacy and tolerability of scalp cooling in patients undergoing (neo)adjuvant chemotherapy for early breast cancer. *Breast Cancer Res Treat*. 2019;173:135-143.
22. Rippe B, Kamiya A, Folkow B. Transcapillary passage of albumin, effects of tissue cooling and of increases in filtration and plasma colloid osmotic pressure. *Acta Physiol Scand*. 1979;105:171-187.
23. Rippe B, Grega GJ. Effects of isoprenaline and cooling on histamine induced changes of capillary permeability in the rat hindquarter vascular bed. *Acta Physiol Scand*. 1978;103:252-262.

24. Ameri H, Chader GJ, Kim JG, et al. The effects of intravitreous bevacizumab on retinal neovascular membrane and normal capillaries in rabbits. *Invest Ophthalmol Vis Sci*. 2007;48(12):5708-5715.
25. Kimoto K, Kubota T. Anti-VEGF agents for ocular angiogenesis and vascular permeability. *J Ophthalmol*. 2012;2012:1-11.
26. Ashina K, Tsubosaka Y, Kobayashi K, et al. VEGF-induced blood flow increase causes vascular hyper-permeability in vivo. *Biochem Biophys Res Commun*. 2015;464(2):590-595.
27. Lachgar S, Moukadiri H, Jonca F, et al. Vascular endothelial growth factor is an autocrine growth factor for hair dermal papilla cells. *J Invest Dermatol*. 1996;106(1):17-23.
28. Gnann LA, Castro RF, Azzalis LA, et al. Hematological and hepatic effects of vascular epidermal growth factor (VEGF) used to stimulate hair growth in an animal model. *BMC Dermatol*. 2013;13:15.
29. Meephansan J, Thummakriengkrai J, Ponnikorn S, et al. Efficacy of topical tofacitinib in promoting hair growth in non-scarring alopecia: possible mechanism via VEGF induction. *Arch Dermatol Res*. 2017;309(9):729-738.
30. Zhang X, Zhou D, Ma T, et al. Vascular endothelial growth factor protects CD200-Rich and CD34-positive hair follicle stem cells against androgen-induced apoptosis through the phosphoinositide 3-Kinase/Akt pathway in patients with androgenic alopecia. *Dermatol Surg*. 2020;46(3):358-368.
31. Gadgeel SM, Stevenson JP, Langer CJ, et al. Pembrolizumab and platinum-based chemotherapy as first-line therapy for advanced non-small-cell lung cancer: Phase 1 cohorts from the KEYNOTE-021 study. *Lung Cancer*. 2018;125:273-281.

SUPPORTING INFORMATION

Additional supporting information may be found online in the Supporting Information section.

How to cite this article: Sagawa N, Oshima Y, Hiratsuka T, Kono Y, Etoh T, Inomata M. Role of increased vascular permeability in chemotherapy-induced alopecia: In vivo imaging of the hair follicular microenvironment in mice. *Cancer Sci*. 2020;111:2146–2155. https://doi.org/10.1111/cas.14396